Supplementary Materials

Novel Photoluminescence and Optical Thermometry of Solvothermally derived Tetragonal $ZrO_2:Ti^{4+},Eu^{3+}$ Nanocrystals

Lu Li[1], Xuesong Qu[1*], Guo-Hui Pan[2*], Jung Hyun Jeong[3*]

[1]*Department of Physics, Changchun Normal University, Changchun 130032, China*

[2]*State Key Laboratory of Luminescence Science and Technology, Changchun Institute of Optics, Fine Mechanics and Physics, Chinese Academy of Sciences, Changchun 130033, China*

[3]*Department of Physics, Pukyong National University, Busan 608-737, Republic of Korea*

To whom correspondence should be addressed: qxs0913@163.com, guohui.pan@aliyun.com, jhjeong@pknu.ac.kr

Table S1. The assignment of the observed emission lines for Eu^{3+} in the t-ZrO_2 NCs and fluorescence decay constants yielded by bi-exponential fitting

Eu^{3+} type	$^5D_0 \rightarrow {}^7F_1$ magnetic dipole transition (nm)	$^5D_0 \rightarrow {}^7F_2$ forced electric dipole transition (nm)	$^5D_0 \rightarrow {}^7F_3$ forbidden transition by the electric dipole and the magnetic dipole (nm)	$^5D_0 \rightarrow {}^7F_4$ forced electric dipole transition (nm)	Fluorescence decay constants (ms)
Eu(I)	592.2	607.0, 628.0, 634.0	652.0, 660.0	714.8	τ_1~6.23, τ_2~2.54
Eu(II)	591.6, 597.2	614.0, 626.4, 631.2	656.2	713.0	τ_1~6.23, τ_2~2.54

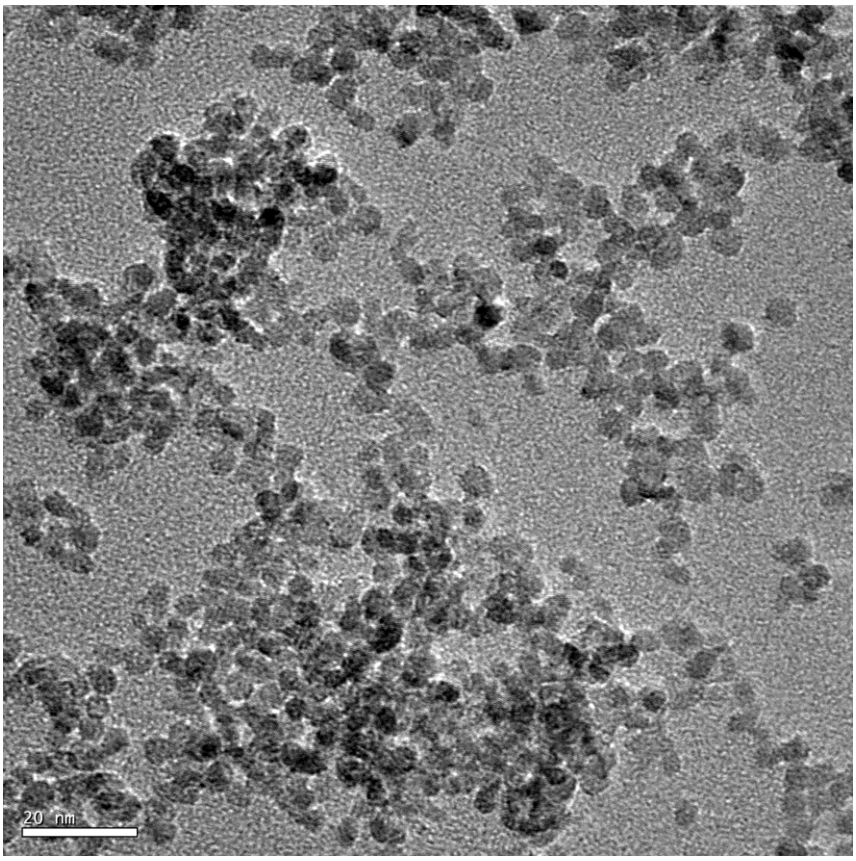

Figure S1. TEM image of t-ZrO_2:4%Ti^{4+},1%Eu^{3+} NCs.

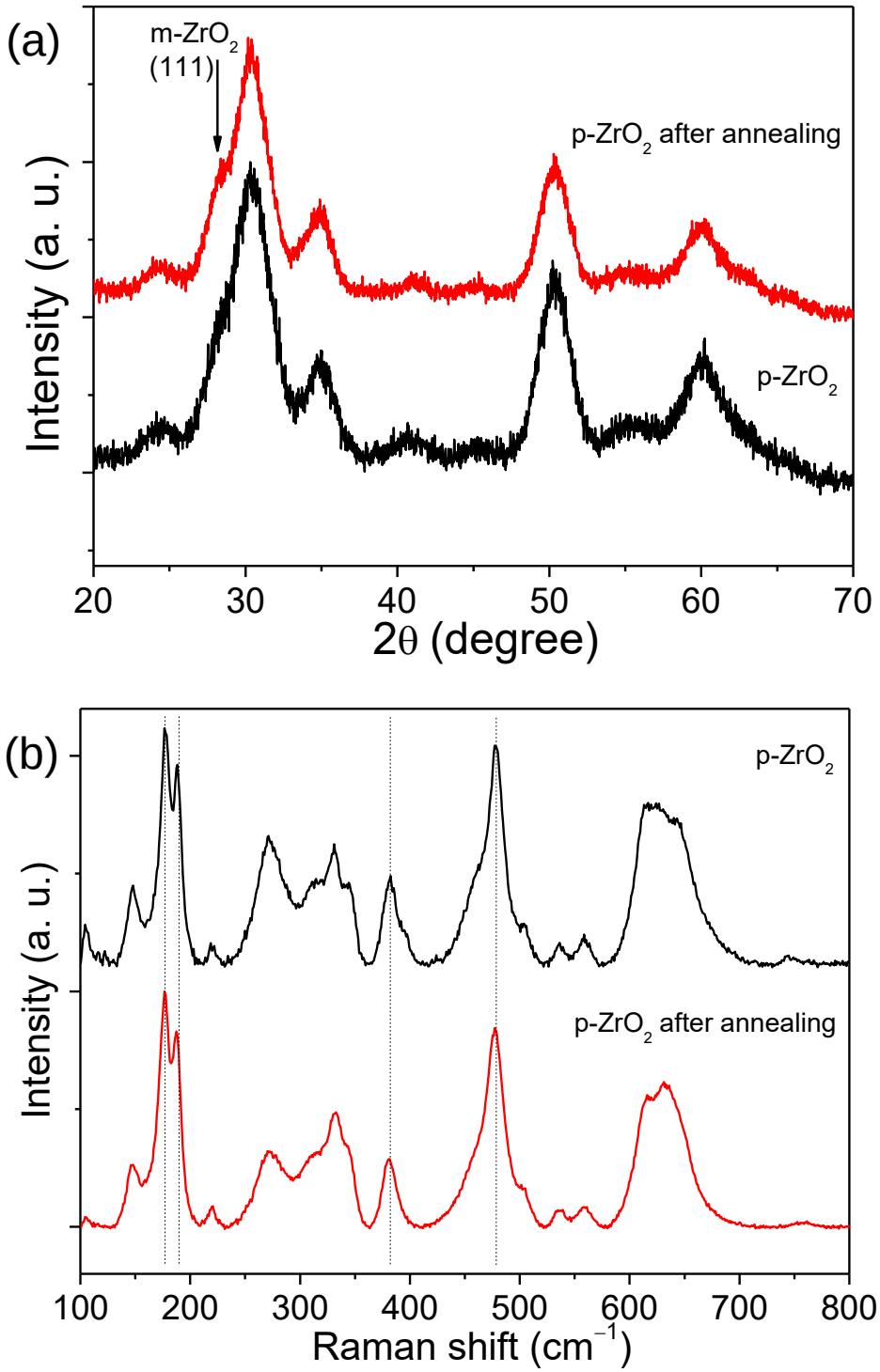

Figure S2. (**a**) Powder XRD patterns and (**b**) Raman spectra of p-ZrO_2 NCs before and after annealing at 400 ^oC; the dash lines in (**b**) indicate the modes of m-ZrO_2.

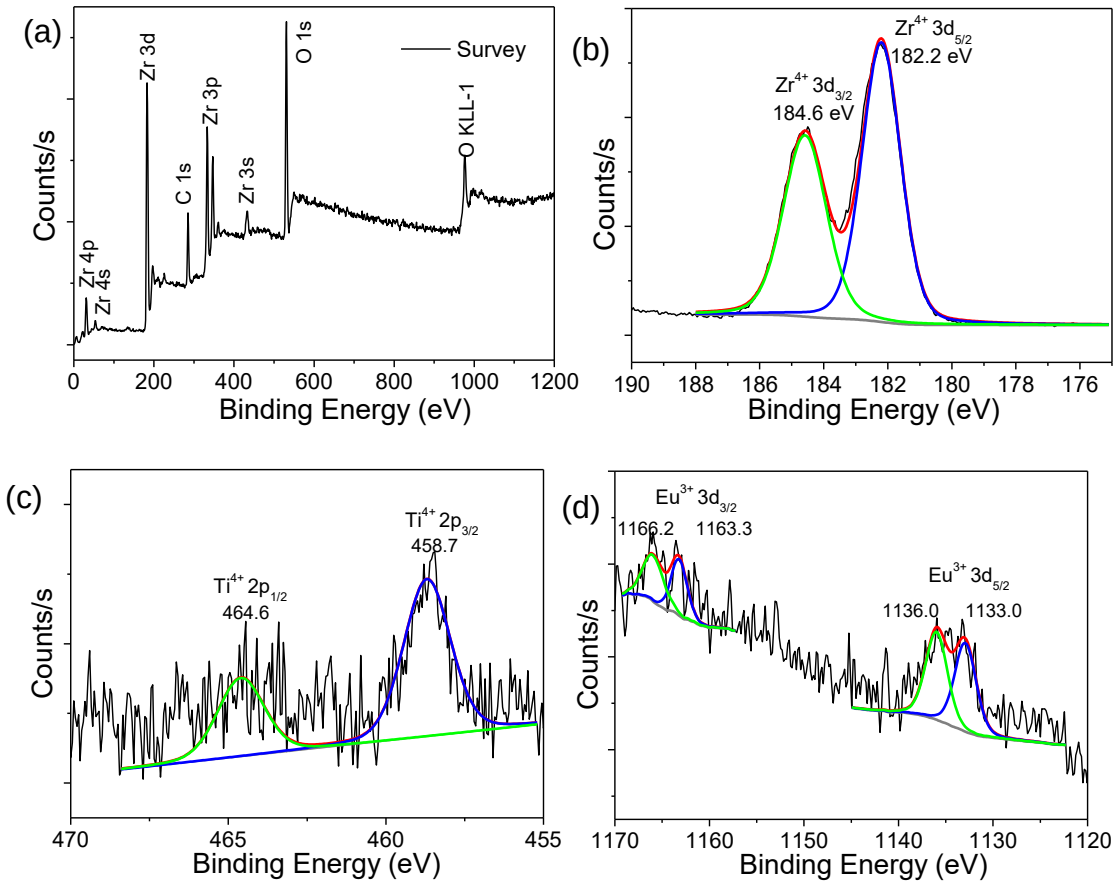

Figure S3. (**a**) XPS survey spectrum of t-ZrO_2:4%Ti^{4+},1%Eu^{3+} NCs and XPS high resolution spectra of (**b**) Zr 3d, (**c**) Ti 2p and (**d**) Eu 3d in t-ZrO_2:4%Ti^{4+},1%Eu^{3+} NCs.

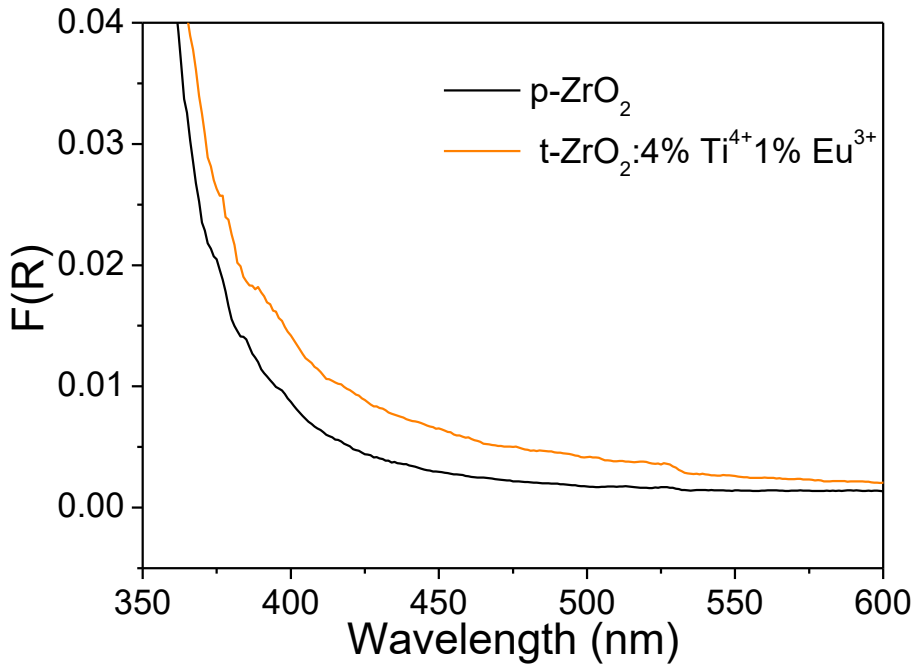

Figure S4. The enlarged diffuse reflection-UV-visible spectra of the as-synthesized p-ZrO_2 and t-ZrO_2:4%Ti^{4+},1%Eu^{3+} NCs in the F(R) range of 0.0–0.04.

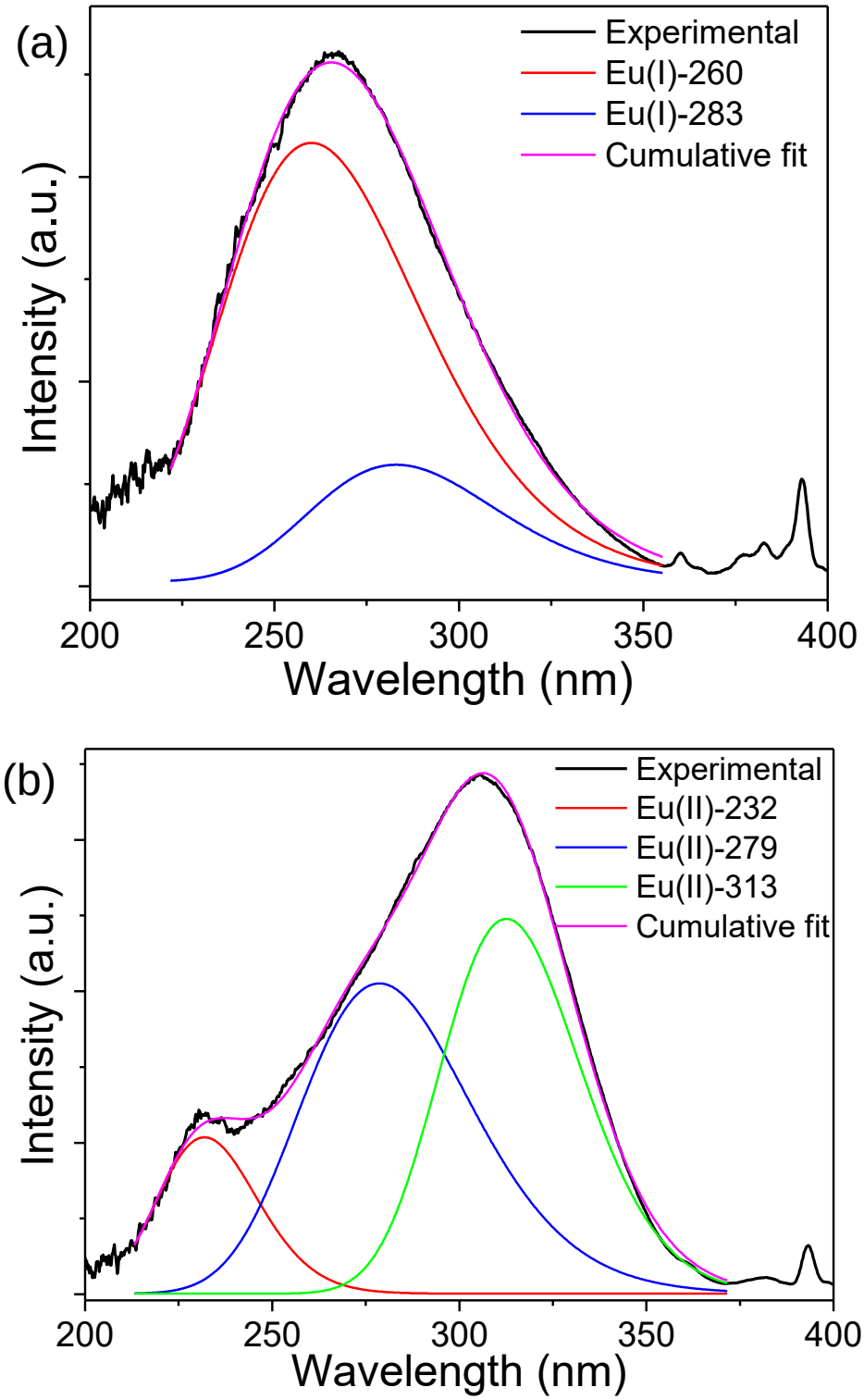

Figure S5. PL excitation spectra of t-ZrO_2:1%Eu^{3+} NCs by monitoring the relative maxima of Eu(I) ((**a**), λ_{em}=607) and Eu(II) ((**b**), λ_{em}= 614 nm) and their spectral decomposition of the corresponding broadband with Gauss typed peaks.

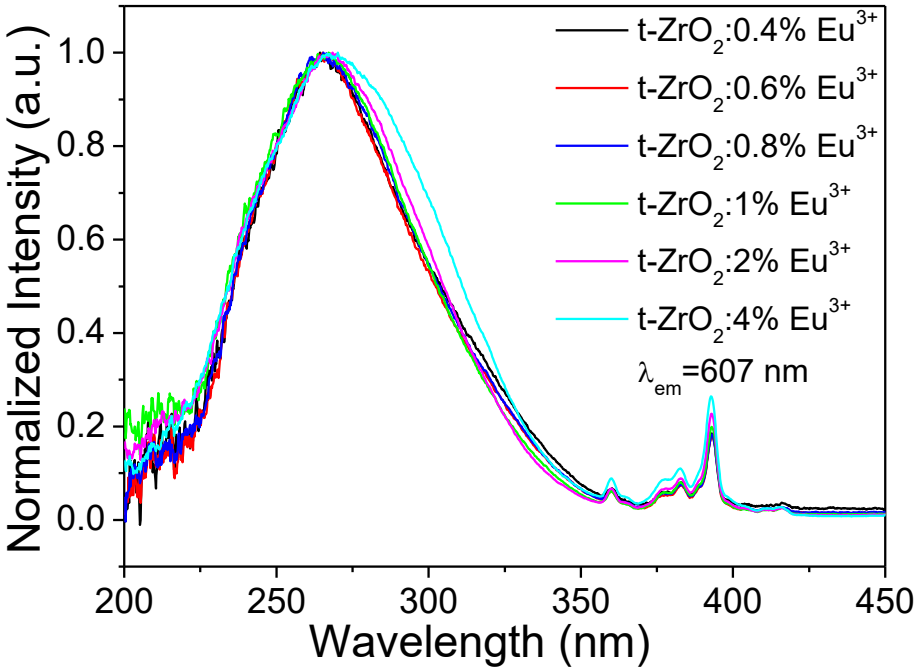

Figure S6. Normalized PL excitation spectra of t-ZrO_2:*x*Eu^{3+} (*x*=0.4%, 0.6%, 0.8%, 1%, 2% and 4%) NCs by monitoring the relative maxima of Eu(I) (λ_{em}=607).

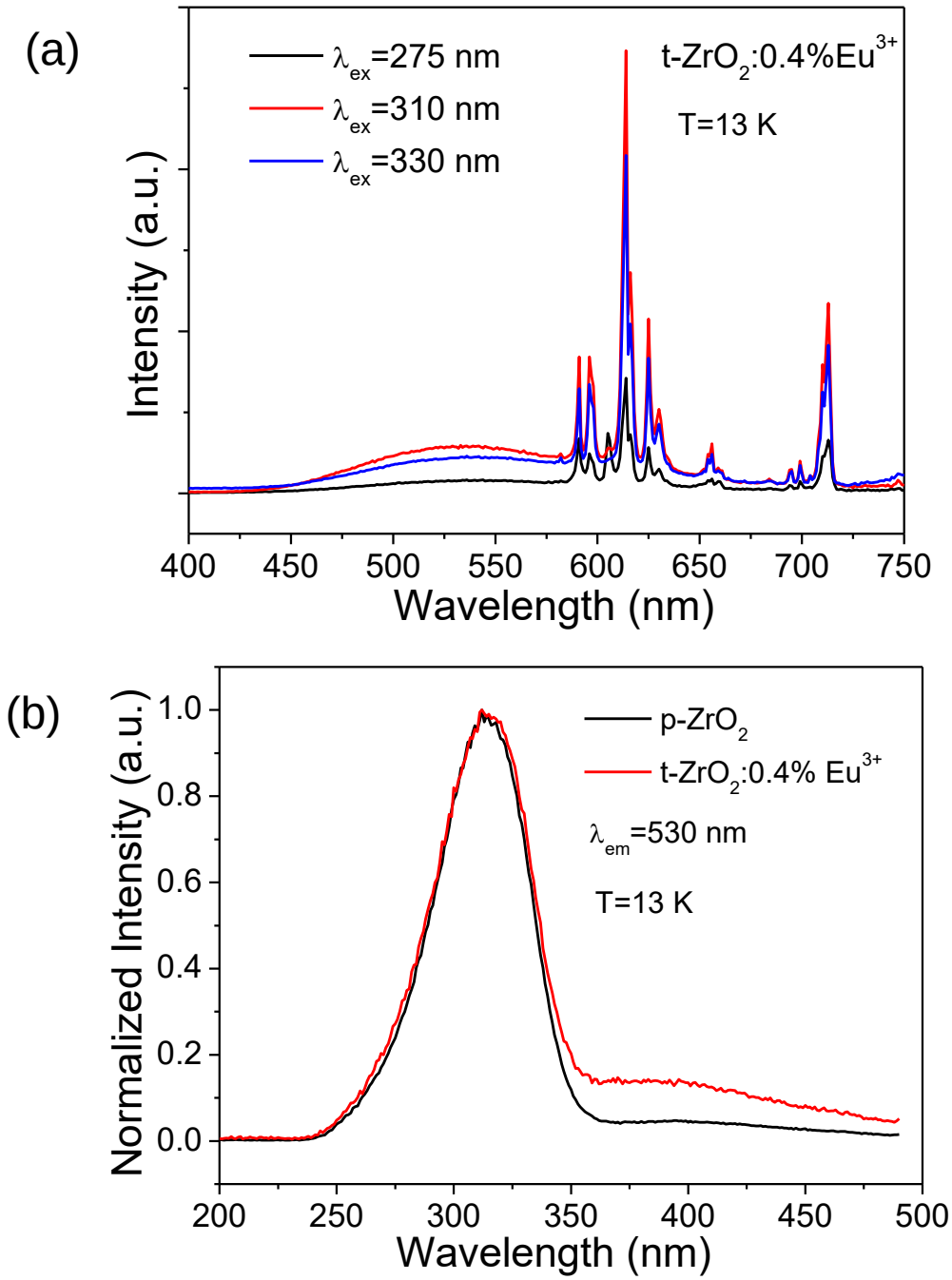

Figure S7. (**a**) The bright broadband PL emissions of CT ($Ti^{3+}\rightarrow O^{-}$) transitions in t-ZrO_2:0.4%Eu^{3+} NCs upon excitation into titanate groups at 13 K, together with the spectral superimposition of stronger sharp line emissions of Eu^{3+} due to nonradiative energy transfer; (**b**) Normalized PL excitation spectra of p-ZrO_2 and t-ZrO_2:0.4%Eu^{3+} NCs upon monitoring the peak of the broadband emissions at 530 nm.

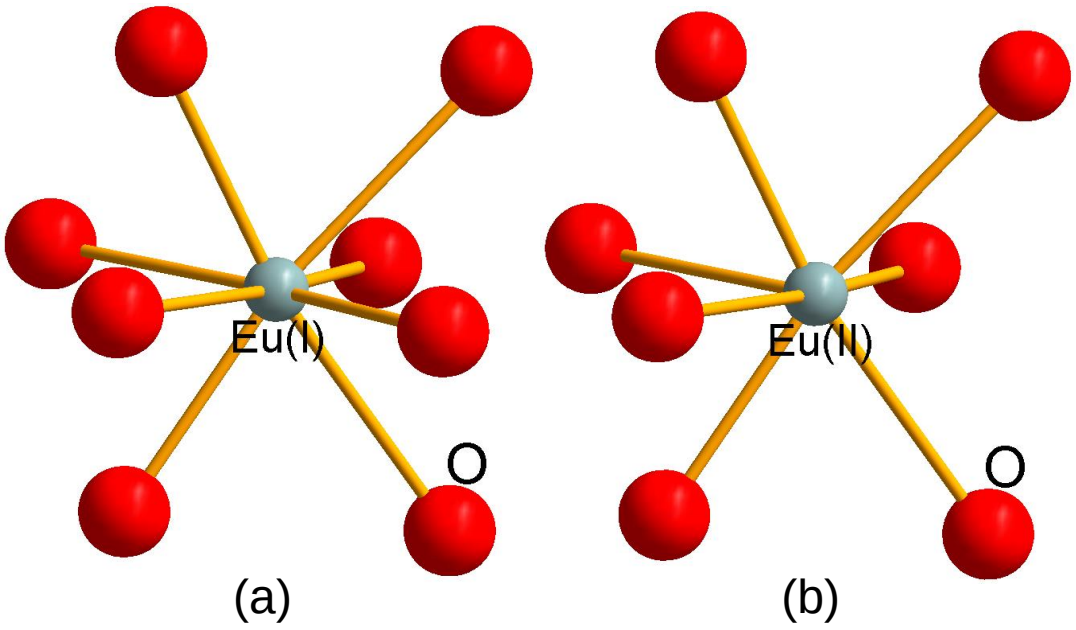

Figure S8. The scheme of oxygen coordination spheres of Eu(I) (a) and Eu (II) (b) in t-ZrO_2 NCs.

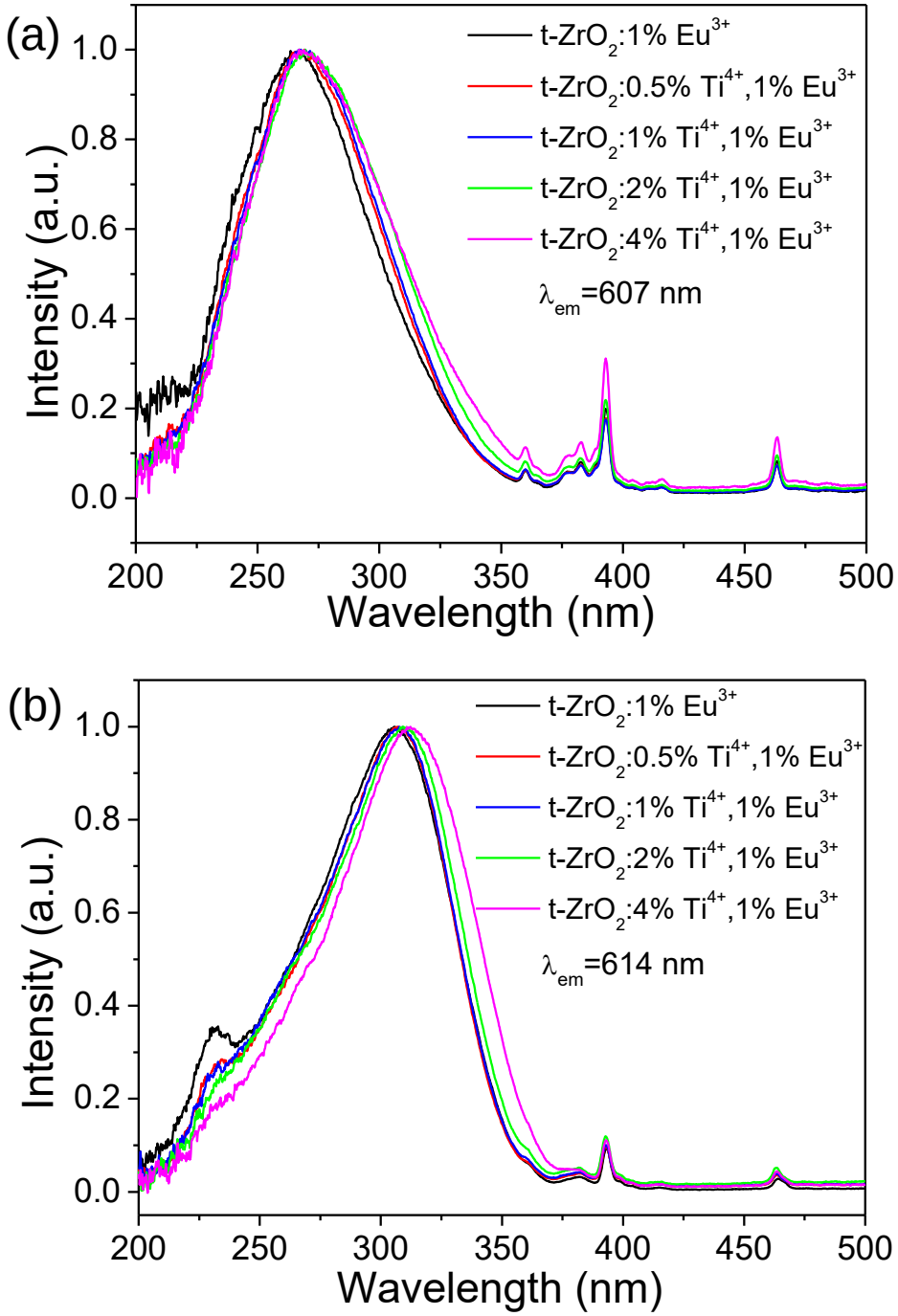

Figure S9. Normalized PL excitation spectra of t-ZrO_2:*x*Ti^{4+},1%Eu^{3+} (*x*=0, 0.5%, 1%, 2% and 4%) NCs by monitoring the relative maxima of Eu(I) ((**a**), λ_{em}=607) and Eu(II) ((**b**), λ_{em}= 614 nm).

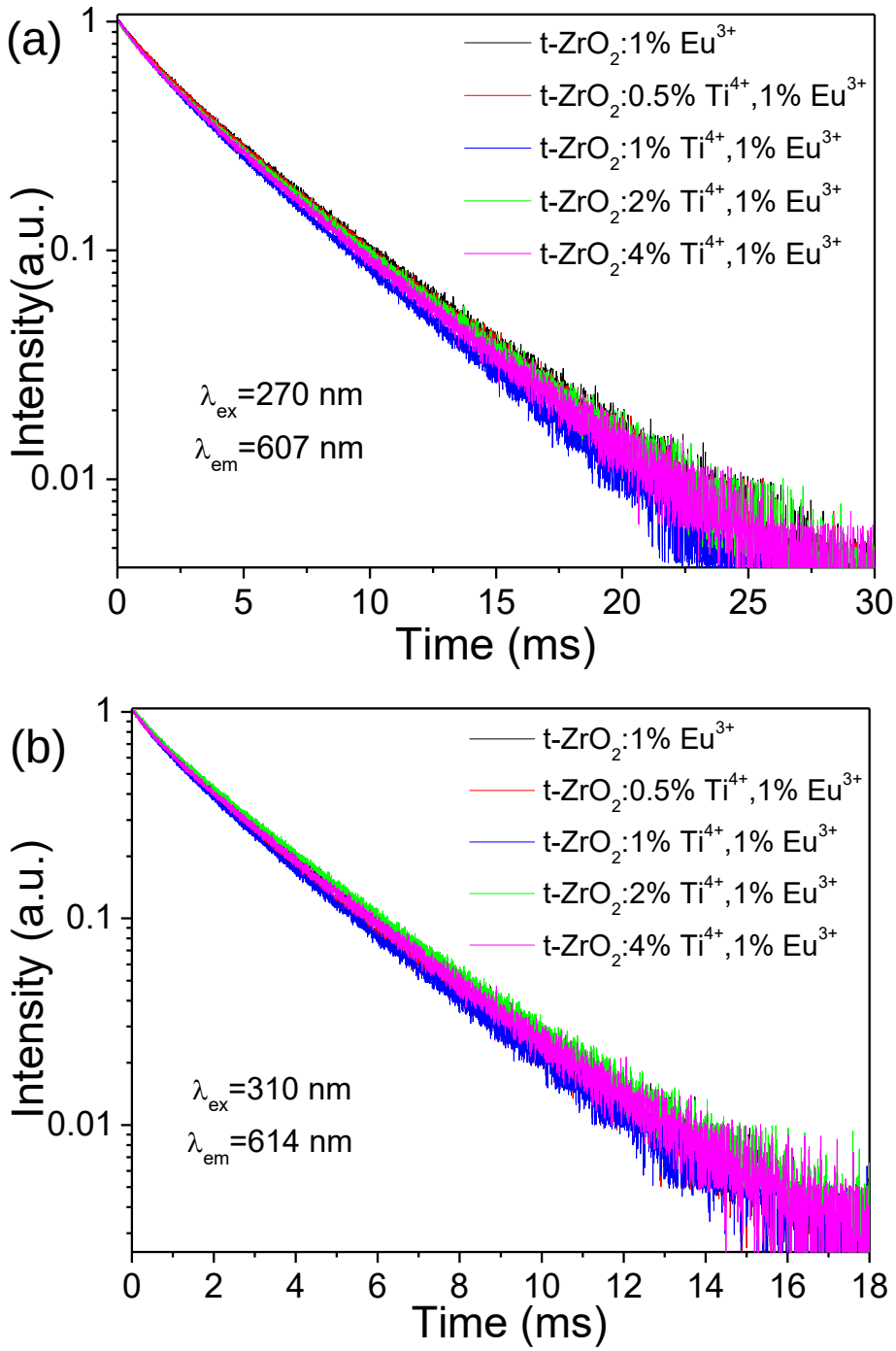

Figure S10. Fluorescence decay traces of t-ZrO_2:*x*Ti^{4+},1%Eu^{3+} (*x*=0, 0.5%, 1%, 2% and 4%) NCs by monitoring the relative maxima of Eu(I) ((**a**), λ_{ex}=270 nm, λ_{em}=607) and Eu(II) ((**b**), λ_{ex}=310 nm, λ_{em}= 614 nm).

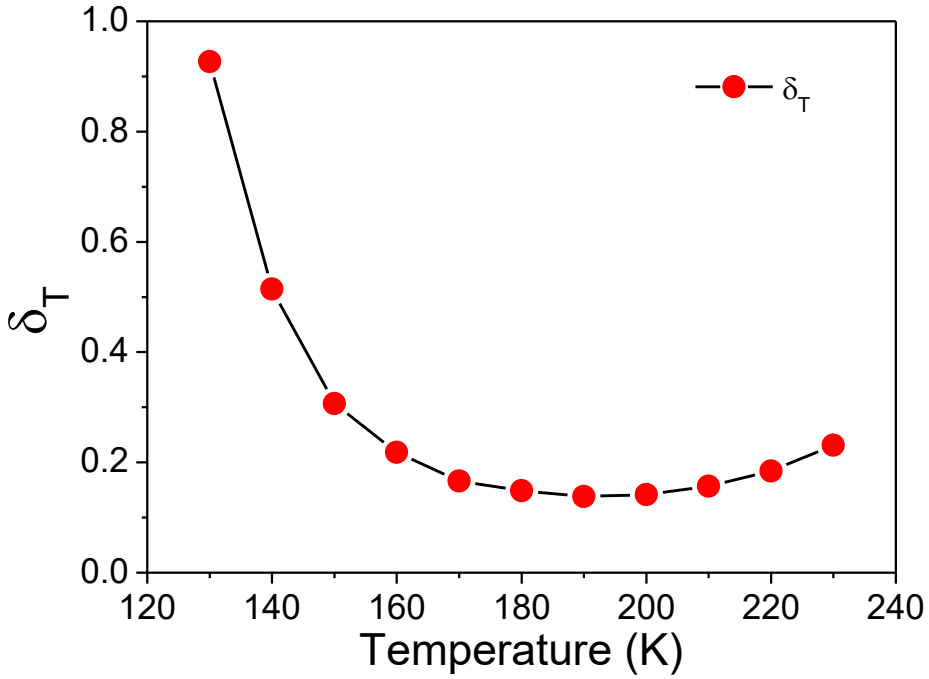

Figure S11. Temperature resolution δ_T of t-ZrO_2:0.4%Eu^{3+} NCs temperature sensing material in the temperature range from 130 to 230 K.

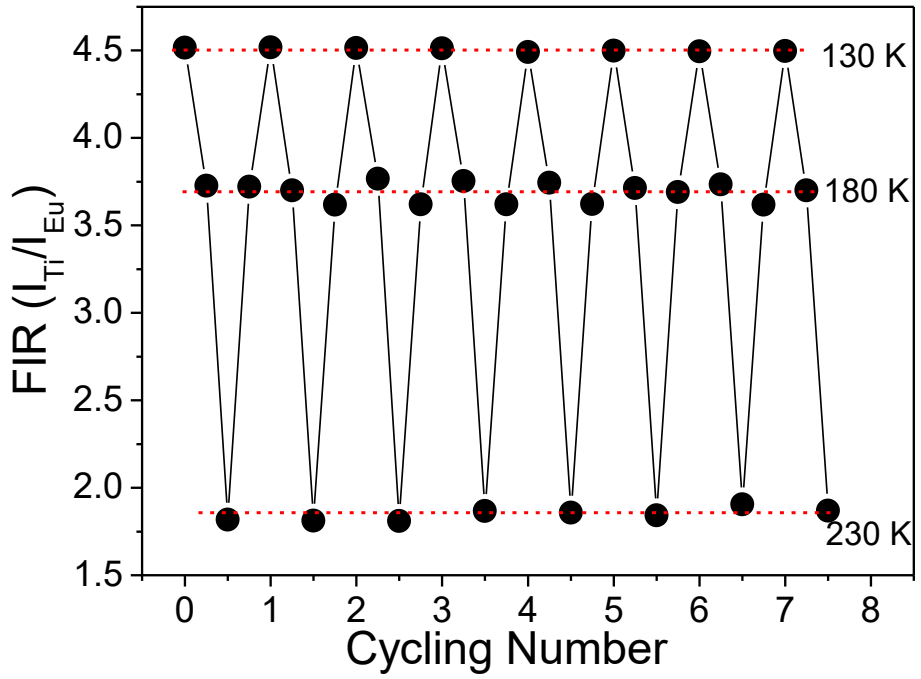

Figure S12. Temperature-induced switching of the FIR between the titanate groups signals (I_{Ti}) (450−580 nm) and Eu^{3+}singals (690–725 nm) (I_{Eu}) (alternating between 130 K and 230 K). The dashed line is drawn to guide the eyes.